

Design of Dual-band Graphene-Based Absorbers by Exciting Graphene Plasmon Polaritons: Circuit Model Analysis

Saeedeh Barzegar-Parizi¹,

¹Electrical Engineering Department, Sirjan University of Technology, Sirjan.

*barzegarparizi@sirjantech.ac.ir

Abstract: This article presents designing two dual-band absorbers based on graphene metasurfaces for terahertz frequencies. The absorbers are composed of one- and two-dimensional (2D) arrays of ribbons and disks deposited on a dielectric film terminated by a metallic back reflector. The design is based on the excitation of the graphene-plasmon polaritons (GPPs) of the patterned array of graphene elements in each resonant band. The analytical circuit model is used to derive the closed-form relations for the geometrical parameters of the absorber and the properties of the graphene. In the circuit model, the graphene patterned array appears as a surface admittance including infinite parallel branches composed of the R-L-C series circuit in which each branch is equivalent to a GPP of the patterned array. Our purpose is the design based on exciting two first GPPs, so we employed two parallel branches including the R-L-C series circuit in the circuit model. The results obtained by the analytical solution are compared to the simulations carried out by HFSS. The agreement between results obtained by HFSS and the circuit model is very good. However, the drawback of full wave simulators is that they are very time-consuming.

1. Introduction

Surface plasmon polaritons (SPPs), the eigenmodes of an interface between a dielectric and metal with strong interaction between light and free electrons, have attracted considerable attention in the past decades [1-3]. They allow overcoming the diffraction limit to focus light into deep-subwavelength volumes with huge field enhancements [2,3]. Plasmonics with fascinating properties has provided promising applications in switches [4,5], demultiplexers [6,7], and photovoltaics [8, 9] based on noble metals in the visible or near-infrared regimes where the noble metals support SPPs. However, the plasmonic devices based on noble metals are constrained because of some their limitations such as poor confinement, the difficulty in controlling their permittivity functions, and high material losses, especially in terahertz (THz) frequencies.

With the discovery of graphene, new knowledge and opportunities have emerged in the field of optoelectronics and photonics devices in the mid-infrared and THz regions [10,11]. Graphene, a one-atom-thick sheet of carbon atoms, has appeared as a novel platform due to its considerable electrical and optical properties, such as high thermal

conductivity [11], Gate-variable optical conductivity [12], controllable plasmonic properties [13] and high-speed operation [14]. Such as noble metals, it is discovered that graphene can be considered as a promising candidate for plasmonic devices. However, in comparison to surface plasmon polaritons in noble metals [15], graphene-plasmon polaritons (GPPs) display strong confinement and relatively longer propagation distance, with the ability in controlling its plasmonic properties electrically or chemically [16-18]. These extraordinary features make graphene a promising material for many applications in optical modulators [19-21], sensors [22-26], and absorbers [27-39]. Recently extensive studies are done on the graphene-based absorbers as broadband, multiband, and resonant absorbers [27-40]. Solar energy harvesting [41,42], refractive index sensors [43], microbolometers [44], thermal imaging [45], thermal IR emitters [46], bio-sensing are some promising applications of absorbers.

In this paper, the patterned array of graphene as one-dimensional ribbons and two-dimensional disks are used to design dual-band absorbers. In our previous works [39,40], we used the graphene and metallic patterned arrays to achieve dual-band absorbers by exciting the fundamental GPPs at both bands. In the present paper, the geometrical parameters and graphene properties (the chemical potential and the relaxation time of graphene) are designed in this way that dual-band absorbers can be realized by exciting different GPPs [33] at each resonant frequency. Furthermore, the resonant bands of the proposed absorbers are very narrow band in comparison to our previous work [39,40] and also, the absorption values between two bands is nearly zero.

We propose a circuit model [47-49] for the proposed devices to extract the parameters of the absorber in the closed-form. Furthermore, the analyze using the analytical circuit model is very fast while the simulation done by the full-wave simulator is very time-consuming. We demonstrate that the absorbers with different resonant frequencies can be designed by the proper design of the geometrical parameters or the properties of graphene. Furthermore, the main advantage of our proposed absorber compared to other works [27] is the simplicity of the structure.

The paper is organized as follows: In Sec. 2, we design a dual-band absorber based on an array of graphene ribbons. The design is done by the analytical circuit model equivalent to the proposed absorber. We extract the closed

form relations for the absorber parameters by exciting two first GPPs of the array of graphene ribbons. Some numerical examples are investigated in this section. In Sec. 3, dual-band absorber is developed based on an array of graphene disks. The design procedure is similar to the approach presented in Sec. 2. Some examples are studied in this section. Finally, conclusions are drawn in Sec.4.

2. Dual-band absorber based on the array of graphene ribbons

Graphene patterned arrays support the Graphene-Plasmon Polariton at terahertz frequency. Therefore, it is one of the best materials for designing THz-wave devices [27-39]. The graphene-based devices can be tunable due to the controllable property of the conductivity surface of the graphene. One of the plasmonic devices based on graphene is absorber. Because of the controllable plasmonic properties of graphene, one can adjust the resonance frequencies of the graphene-based absorbers by the Fermi level adjusting of graphene without need to change the geometrical parameters of the structure.

Most absorbers are commonly composed of three layers: a metamaterial deposited on a dielectric film terminated by a metallic back reflector. The top metamaterial layer contains patterned arrays of one-dimensional or two-dimensional subwavelength elements. To prevent the wave transmission, the thickness of the bottom metal film should be thick enough. The absorption is calculated as $A(\omega) = 1 - R(\omega) - T(\omega)$, in which $T(\omega) = |S_{21}|^2$ and $R(\omega) = |S_{11}|^2$ are the transmission and reflection coefficients, respectively. Since the bottom metal film avoids the penetration of the electromagnetic waves into the structure, the transmission coefficient would be close to zero. Hence, the absorption is calculated as $A(\omega) = 1 - R(\omega)$.

For the development of EM absorber in the low terahertz regime, many have used the graphene-based patterned arrays as a top metamaterial layer in a Salisbury absorber. In this paper, two dual-band absorbers based on the array of graphene ribbons and disks are designed. The absorbers are realized by exciting the GPPs in the graphene patterned arrays.

In [47] and [48], the graphene-plasmon polaritons are surveyed in the arrays of graphene ribbons and disks, respectively. In these papers, the eigenvalues and eigenfunctions corresponding to the GPPs are analytically extracted. In the present paper, we design the geometrical parameters of the absorber and the properties of graphene to excite the first and second GPPs to achieve a dual-band absorber with absorption near to one. The results obtained by analytical solutions are compared to those obtained by simulation carried out by HFSS. At the first step, we survey the absorber based on the one-dimensional array of ribbons. At the second step, the results related to the two-dimensional array of disks are investigated. The most important advantage of these absorbers is their simplicity.

Suppose the configuration of the absorber as shown in Fig. 1. The structure includes three layers as: the top layer of the graphene ribbon array, the middle layer of the dielectric film and the bottom layer as a thick enough metallic film. The width of ribbons is w which periodically arranged

along the x -direction with the period L . The ribbons are infinite in the y -direction. The thickness and the refractive index of the dielectric film are h and n_s , respectively. Note that the refractive index of the dielectric film is considered as $n_s = 3.13$ during the paper. This refractive index corresponds to Al_2O_3 .

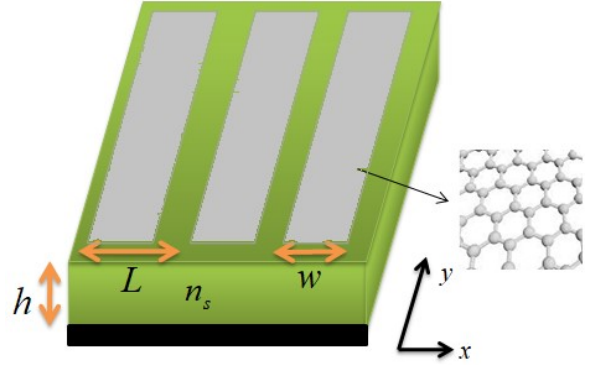


Fig. 1. Structure of EM absorber based on an array of graphene ribbons with width w and period L placed above a dielectric layer with thickness h and refractive index n_s terminated by a metallic film which acts as a back reflector.

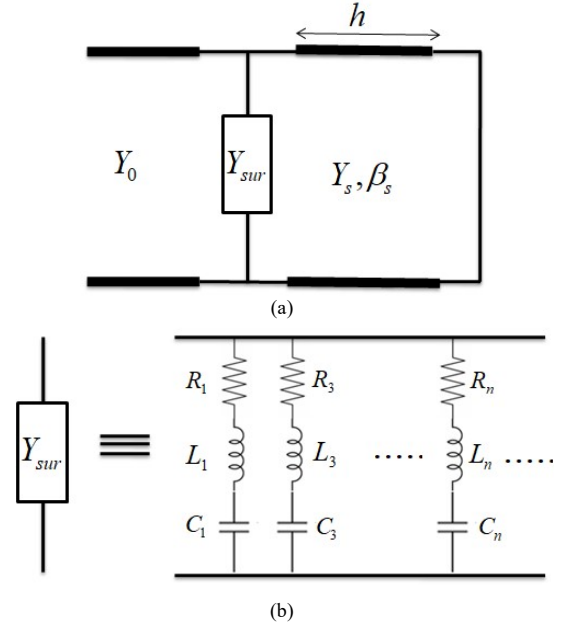


Fig. 2. (a) The equivalent circuit model for the proposed absorber (b) the parallel branches composed of the R-L-C series circuit corresponding to the surface admittance equivalent to the array of the ribbons.

The surface conductivity of graphene [48] is given by:

$$\sigma_g = \frac{2e^2 k_B T}{\pi \hbar^2} \frac{j}{-\omega + j\tau^{-1}} \ln[2 \cosh(E_F / 2k_B T)] - \frac{je^2}{4\pi \hbar} \ln \left[\frac{2E_F - \hbar(\omega - j\tau^{-1})}{2E_F + \hbar(\omega - j\tau^{-1})} \right] \quad (1)$$

Where e is the electron charge, E_F denotes the Fermi level, \hbar refers to the reduced Plank constant, k_B represents the

Boltzmann constant, $\omega = 2\pi f$ shows the angular frequency, $T = 300$ K is the temperature, and τ is the relaxation time. The surface conductivity of graphene contains intraband conductivity (first term in (1)) and interband conductivity (the second term in (1)).

Suppose the proposed absorber illuminated by a TM polarized plane wave. The equivalent circuit model for the absorber plotted in Fig.1 is demonstrated in Fig. 2(a). In this circuit, the ribbon array illuminated by a normally incident plane wave can be modeled by a surface admittance [47] as:

$$Y_{sur} = \sum_{n=1(\text{odd})}^{\infty} \frac{S_n^2}{L} (\sigma_g^{-1} + \frac{q_n}{2j\omega\epsilon_{eff}})^{-1} \quad (2)$$

Where

$$S_n = \int_{-w/2}^{w/2} \psi_n(x) dx \quad (3)$$

in which $\psi_n(x)$ and q_n are the n 'th normalized eigenfunction and eigenvalue corresponding to n 'th the resonant modes excited by the array of the ribbons. The eigenfunctions and eigenvalues have been calculated in [47]. In (1), $\epsilon_{eff} = \epsilon_0(1 + n_s^2)/2$. It is worth to describe that the

even modes don't appear in (2), since the values of S_n are zero for even modes. The surface admittance presented in (2) can be considered as the parallel branches composed of the R-L-C series circuit corresponding to each GPPs shown as Fig. 2(b):

$$Y_{sur} = \sum_{n=1(\text{odd})}^{\infty} (R_n + jL_n\omega + \frac{1}{jC_n\omega})^{-1} \quad (4)$$

in which the values of R_n , L_n and C_n are calculated as:

$$R_n = \frac{L}{S_n^2} \text{Re}\{\sigma_g^{-1}\}, L_n = \frac{L}{S_n^2} \frac{\text{Im}\{\sigma_g^{-1}\}}{\omega}, C_n = \frac{S_n^2}{L} \frac{2\epsilon_{eff}}{q_n} \quad (5)$$

In this paper, our aim is the design of the geometrical parameters and graphene properties to excite two first GPPs. Therefore $n=1$ and $n=3$ are appeared in (2). The eigenfunctions corresponding to these modes are calculated as:

$$\begin{aligned} \psi_1(x) &= w^{-\frac{1}{2}} \left[1.2 \sin(\cos^{-1}(\frac{2x}{w})) - 0.106 \sin(3 \cos^{-1}(\frac{2x}{w})) \right] \\ \psi_3(x) &= w^{-\frac{1}{2}} \left[0.308 \sin(\cos^{-1}(\frac{2x}{w})) + 1.19 \sin(3 \cos^{-1}(\frac{2x}{w})) \right. \\ &\quad \left. - 0.484 \sin(5 \cos^{-1}(\frac{2x}{w})) \right] \end{aligned} \quad (6)$$

where the corresponding eigenvalues are specified in Table. II of [47] for different filling factor (w/L).

In the equivalent circuit model (Fig. 2 (a)), $\beta_s = k_0 n_s$ and $Y_s = n_s / \eta_0$ are the propagation constant and the admittance of transmission line corresponding to the dielectric slab respectively, where $\eta_0 = 120\pi$ is the free-space impedance and $k_0 = \omega/c$ (c is the speed of light) is the wavenumber of free space. The metallic back reflector can be approximately considered as a short circuit. So, the input admittance of the device is obtained as:

$$Y_{in} = Y_{sur} - jY_s \cot(\beta_s h) \quad (7)$$

Our purpose is designing a dual-band absorber by exciting the GPPs at each band. Therefore, the input admittance of the absorber can be written as:

$$\begin{aligned} Y_{in} &= (R_1 + jL_1\omega + \frac{1}{jC_1\omega})^{-1} + \\ &\quad (R_3 + jL_3\omega + \frac{1}{jC_3\omega})^{-1} - jY_s \cot(\beta_s h) \end{aligned} \quad (8)$$

For the first band (lower frequencies), the second term of the right side in (8) can be omitted for the input admittance. Hence, we have

$$\begin{aligned} Y_{in} |_{\omega=\omega_1} &= (R_1 + jL_1\omega_1 + \frac{1}{jC_1\omega_1})^{-1} \\ &\quad - jY_s \cot(\beta_s h) |_{\omega=\omega_1} \end{aligned} \quad (9)$$

But, however, it is necessary to consider the surface admittance of the first GPPs at the second band:

$$\begin{aligned} Y_{in} |_{\omega=\omega_2} &= (R_1 + jL_1\omega_2 + \frac{1}{jC_1\omega_2})^{-1} \\ &\quad + (R_3 + jL_3\omega_2 + \frac{1}{jC_3\omega_2})^{-1} - jY_s \cot(\beta_s h) |_{\omega=\omega_2} \end{aligned} \quad (10)$$

To design a dual-band absorber, we consider the below conditions at the second band:

$$\beta_s h |_{\omega=\omega_2} = \pi/2 \quad (11.a)$$

$$L_3 C_3 = \frac{1}{\omega_2^2} \quad (11.b)$$

$$R_3 = \eta_0 / \alpha \quad (11.c)$$

We define the parameter α in the following. At appropriately low frequencies (where the inter-band term of conductivity is dominant) and for $E_F \gg k_B T$, σ_g will be of the Drude form:

$$\sigma_g = \frac{e^2 E_F \tau}{\pi \hbar^2} \frac{1}{1 + j\omega\tau} \quad (12)$$

The values of R, L, and C are obtained as:

$$R_n = \frac{L}{S_n^2} \frac{\pi \hbar^2}{e^2 E_F \tau}, L_n = \tau R_n, C_n = \frac{S_n^2}{L} \frac{2\epsilon_{eff}}{q_n} \quad (13)$$

Therefore, (11) leads to:

$$h = \frac{c}{4n_s f_2} \quad (14.a)$$

$$w = \frac{e^2 E_F r_3}{2\pi \hbar^2 \epsilon_{eff} \omega_2^2} \quad (14.b)$$

$$\tau E_F = \alpha \frac{L}{w} \frac{\pi \hbar^2}{\varsigma_3 e^2 \eta_0} \quad (14.c)$$

in which, $r_n = q_n w$ which depends on the filling factor (w/L) and $\varsigma_n = S_n^2 / w$. (with $\varsigma_1 = 0.88$, $\varsigma_3 = 0.0573$) Hence, according to (11), the input admittance of the second band (10) would be as:

$$Y_{in} |_{\omega=\omega_2} = (R_1 + jL_1\omega_2 + \frac{1}{jC_1\omega_2})^{-1} + \frac{1}{R_3} \quad (15)$$

Using $L_1 C_1 = \frac{r_3}{r_1 \omega_1^2}$ and $L_1 = \tau R_1$, Eq. (15) can be

rewritten as:

$$Y_{in}|_{\omega=\omega_2} = \frac{1}{R_3} \left(1 + \frac{R_3 \left(1 - j\tau\omega_2 \left(1 - \frac{r_1}{r_3} \right) \right)}{R_1 \left(1 + \tau^2 \omega_2^2 \left(1 - \frac{r_1}{r_3} \right)^2 \right)} \right) \quad (16)$$

To achieve the absorption above 95%, $|S_{11}|^2 < 0.05$ should be satisfied, so

$$|S_{11}| = \left| \frac{1 - Y_{in}\eta_0}{1 + Y_{in}\eta_0} \right| < 0.22 \quad (17)$$

For the second band, using $\frac{R_3}{R_1} = \frac{S_1^2}{S_3^2}$ and $R_3 = \eta_0 / \alpha$,

(17) leads to:

$$\left| \frac{1 - \frac{S_1^2 \left(1 - j\tau\omega_2 \left(1 - \frac{r_1}{r_3} \right) \right)}{S_3^2 \left(1 + \tau^2 \omega_2^2 \left(1 - \frac{r_1}{r_3} \right)^2 \right)} + 1}{1 + \frac{S_1^2 \left(1 - j\tau\omega_2 \left(1 - \frac{r_1}{r_3} \right) \right)}{S_3^2 \left(1 + \tau^2 \omega_2^2 \left(1 - \frac{r_1}{r_3} \right)^2 \right)} + 1} \alpha \right| < 0.22 \quad (18)$$

Therefore, the parameter of α prepares the absorption above 95% at the second band.

Now, we impose the conditions to achieve perfect absorption at first frequency:

$$\text{Im}(Y_{in})|_{\omega=\omega_1} = 0 \quad (19.a)$$

$$\text{Re}(Y_{in})|_{\omega=\omega_1} = 1/\eta_0 \quad (19.b)$$

Therefore, we have

$$\frac{L_1 \omega_1 \left(1 - \frac{1}{L_1 C_1 \omega_1^2} \right)}{R_1^2 + L_1^2 \omega_1^2 \left(1 - \frac{1}{L_1 C_1 \omega_1^2} \right)^2} + Y_s \cot(\beta_s h)|_{\omega=\omega_1} = 0 \quad (20.a)$$

$$\frac{R_1}{R_1^2 + L_1^2 \omega_1^2 \left(1 - \frac{1}{L_1 C_1 \omega_1^2} \right)^2} = 1/\eta_0 \quad (20.b)$$

Using $L_1 C_1 = \frac{r_3}{r_1 \omega_1^2}$, $R_3 = \eta_0 / \alpha$ and $L_1 = \tau R_1$, Eqs. (20)

can be rewritten as:

$$\tau \omega_1 \left(1 - \frac{r_1 \omega_1^2}{r_3 \omega_1^2} \right) = -n_s \cot(\beta_s h)|_{\omega=\omega_1} \quad (21.a)$$

$$\left(\tau \omega_1 \left(1 - \frac{r_1 \omega_1^2}{r_3 \omega_1^2} \right) \right)^2 = \frac{\alpha R_3}{R_1} - 1 \quad (21.b)$$

leading to

$$(n_s \cot(\beta_s h)|_{\omega=\omega_1})^2 = \frac{\alpha S_1^2}{S_3^2} - 1 \quad (22)$$

So, the ratio of the first resonant frequency to the second one is constant and can be extracted as:

$$\frac{\omega_1}{\omega_2} = \frac{2}{\pi} \cot^{-1} \left(\frac{1}{n_s} \sqrt{\frac{\alpha S_1^2}{S_3^2} - 1} \right) \quad (23)$$

To design a dual-band absorber, we consider a specified value for the second band frequency (ω_2). Using (18), (23) and (21), we determine the proper value for the parameter of α , the first resonant frequency and the relaxation time of graphene. Note that r_1 and r_3 in (18) should be specified, therefore it is necessary to consider a given value for filling factor (w/L). After computing the relaxation time of graphene, the Fermi level can be extracted using (14.b). At the end, the width of ribbons and period are respectively computed by (15.a) and the specified value for the filling factor.

It is worth to describe that there are limitations for selecting the Fermi level (0-1 eV). Furthermore, the relation between the relaxation time and the Fermi level can be described as

$$\tau = \frac{E_f \mu}{e v_f^2} \quad [37], \text{ in which } \mu \text{ is the electron mobility}$$

ranging from about 0.03 m²/Vs to 20 m²/Vs depending on the fabrication process [50-53] and $v_f = 10^6$ m/s is the Fermi velocity. Hence, the electron mobility range restricts the Fermi level selection.

In the following, the parameters of the structure are designed to achieve the dual-band absorbers. We want to design the absorbers with the second resonant frequency as $f_2 = 3\text{THz}$, $f_2 = 4\text{THz}$ and $f_2 = 5\text{THz}$. Table. I show the designed parameters for proposed absorbers in which the filling factor is considered as $w/L = 0.6$ and $\alpha = 1$. For this filling factor, $r_1 = 0.62\pi$ and $r_3 = 2.735\pi$ according to Table. II of [47]. Fig.3 shows the absorption spectra for the designed absorbers. The result obtained the analytical model is compared with the result obtained by full-wave simulations (HFSS), which are in a good agreement. For full-wave simulations conducted by HFSS, graphene is modeled by a layer of thickness $\Delta = 1\text{nm}$ whose permittivity is $\epsilon_g = \epsilon_0 - j\sigma_g/(\Delta\omega)$. As observed, the proposed absorbers are very narrow band at both bands.

Now, we survey the power loss density distributions at two absorption bands. Fig. 4 (a) and (b) show the loss distributions on ribbons at first and second resonant frequencies, respectively. It is clear two first GPPs are excited at resonant frequencies. Of course, the GPP at second resonant frequency corresponds to the third eigenfunction in the array of the ribbons. At first band, the loss distribution is focused at the center of the ribbon and decrease at the sides of the ribbons. For the second band as shown in Fig. 4(b), the loss concentrations would be at areas

around three points (the center and two sides of the center). Note that the loss distributions are uniform in the y-direction.

Table. I: The parameters of the dual-band proposed absorbers

f_2 (THz)	f_1 (THz)	τ (ps)	E_f (eV)	h (μm)	w (μm)	L (μm)
3	1.32	2.64	0.25	8	7.4	12.3
4	1.76	2	0.33	6	5.5	9.2
5	2.2	1.6	0.41	4.8	4.4	7.4

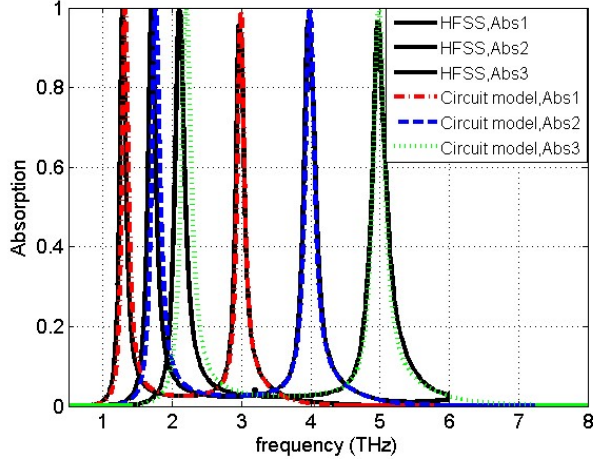


Fig. 3. Absorption spectra of the absorber based on graphene ribbon array with parameters presented in Table. I.

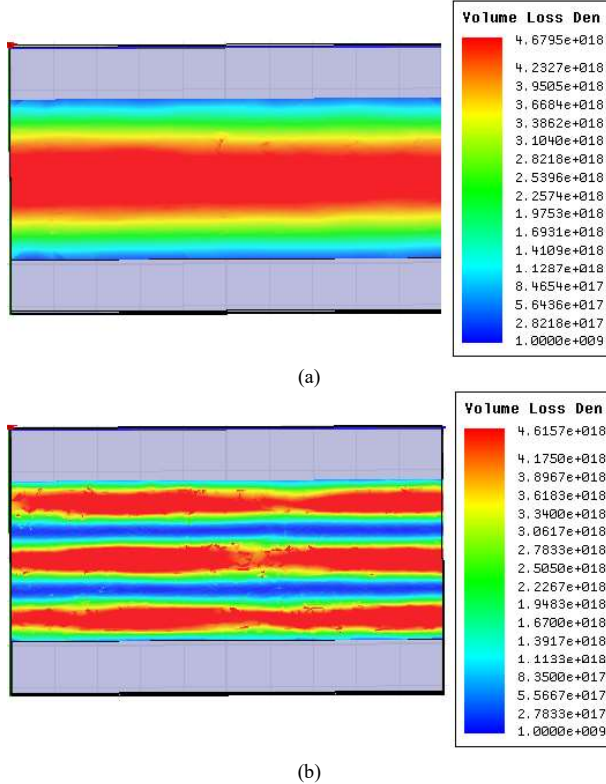


Fig. 4 The loss density distributions on the graphene ribbon at resonant frequencies. (a) first and (b) second resonant band.

In the next step, the influence of the Fermi level changes is investigated as plotted in Fig. 5. The results show that the absorbance firstly increases and then decrease when the values of the Fermi level increases. However, changing the absorption peak of the first band is significant. Furthermore,

the location of the second resonant frequency changes considerably by alerting the Fermi level whereas the first resonant frequency is shifted slightly.

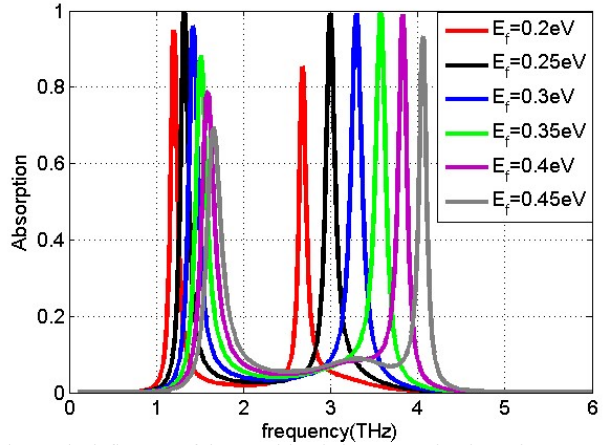


Fig. 5. The influences of the Fermi level changes on the absorption spectra of the absorber 1 presented in Table. I.

The proposed absorber is applicable for TM polarization. Since the array of the ribbons is inductive for TE polarization and due to the fact that the grounded dielectric slab below array is also inductive in the whole the input impedance will be inductive, and thus resonance conditions cannot be expected. Therefore the proposed absorber is sensitive to polarization. To realize the absorber insensitive to polarization, it is necessary to use the two-dimensional patterned array. For normal incident EM waves, because its structure is symmetric, the absorber would be insensitive to polarization. In the next section, the absorber based on graphene disks array is investigated. We demonstrate the absorber based on graphene disks is wide angle and polarization insensitive.

3. Dual-band absorber based on the array of graphene disks

In this section, we study the absorber based on graphene disks. Let us consider an array of graphene disks placed on a dielectric slab terminated by a back reflector as illustrated in Fig. 6. The periods of the structure in the x - and y -directions are L and the radius of the graphene disk is a .

The circuit model equivalent to the proposed absorber is demonstrated in Fig. 2 in which the surface admittance equivalent to the array of disks is analytically computed as [48]:

$$Y_{sur} = \frac{\pi^2}{L^2} \sum_{n=1}^{\infty} \frac{S_n^2}{K_n^2} (\sigma_g^{-1} + \frac{q_{1n}}{j\omega\epsilon_{eff}})^{-1} \quad (24)$$

where

$$S_n = \int_0^a \left[\frac{df_{1n}(\rho)}{d\rho} \rho + f_{1n}(\rho) \right] d\rho \quad (25)$$

with $f_{1n}(\rho)$ given in [48],

$$K_1 = \int_S \xi_{1n} \cdot \xi_{1n}^* dS \quad (26)$$

with $\xi_{1n} = \nabla[f_{1n}(\rho) \cos \varphi]$ and S is the surface of a disk. q_{1n} is the eigenvalue of the equation governing the current on the disks presented in [48] for different $2a/L$. Two first eigenfunctions are computed by:

$$\begin{aligned} f_{11}(\rho) &= [J_1(\xi_{11}\rho/a) - 0.06J_1(\xi_{12}\rho/a) + \\ &\quad 0.022J_1(\xi_{13}\rho/a)] \\ f_{12}(\rho) &= [-0.25J_1(\xi_{11}\rho/a) - 0.965J_1(\xi_{12}\rho/a) + \\ &\quad 0.085J_1(\xi_{13}\rho/a)] \end{aligned} \quad (27)$$

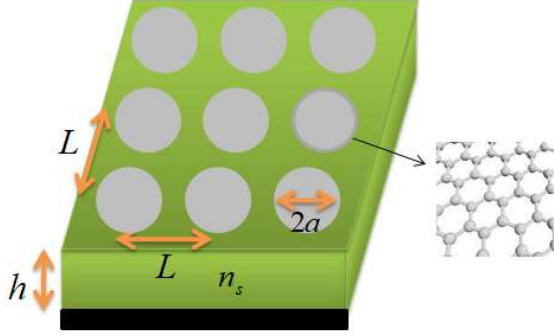


Fig. 6. The configuration of EM absorber composed of an array of graphene disks with radius a and period L placed above a dielectric layer with thickness h and refractive index n_s terminated by a back reflector.

The surface admittance presented in (24) can be considered as the parallel branches composed of the R-L-C series circuit (see Fig. 2(b)) corresponding to each GPPs on disks. The values of R_n , L_n and C_n are calculated as:

$$R_n = \frac{L^2}{\pi^2} \frac{K_n}{S_n^2} \text{Re}\{\sigma_g^{-1}\}, L_n = \frac{L^2}{\pi^2} \frac{K_n}{S_n^2} \frac{\text{Im}\{\sigma_g^{-1}\}}{\omega}, C_n = \frac{\pi^2}{L^2} \frac{S_n^2}{K_n} \frac{\epsilon_{eff}}{q_{1n}} \quad (28)$$

Following the design process in the previous section, the resonant frequencies are related by:

$$\frac{\omega_1}{\omega_2} = \frac{2}{\pi} \cot^{-1} \left(\frac{1}{n_s} \sqrt{\frac{\alpha S_1^2 K_2}{S_2^2 K_1}} - 1 \right) \quad (29)$$

in which $S_1 = 0.612a$, $S_2 = 0.2302a$, $K_1 = 1.2891$ and $K_2 = 4.96$. The relaxation time of graphene computed as:

$$\tau = \frac{-n_s \cot(\beta_s h)|_{\omega=\omega_1}}{\omega_1 (1 - \frac{r_{11}\omega_2^2}{r_{12}\omega_1^2})} \quad (30)$$

in which $r_{1n} = q_{1n}a$. For a specified value of the parameter α , the frequency of the first band and the relaxation time of graphene are computed by (29) and (30). However, it is necessary to survey below condition to achieve the absorption above 95% at the second band:

$$\left| \frac{1 - \left(\frac{K_2 S_1^2 \left(1 - j\tau\omega_2 \left(1 - \frac{r_{11}}{r_{12}} \right) \right)}{K_1 S_2^2 \left(1 + \tau^2 \omega_2^2 \left(1 - \frac{r_{11}}{r_{12}} \right)^2 \right)} + 1 \right) \alpha}{1 + \left(\frac{K_2 S_1^2 \left(1 - j\tau\omega_2 \left(1 - \frac{r_{11}}{r_{12}} \right) \right)}{K_1 S_2^2 \left(1 + \tau^2 \omega_2^2 \left(1 - \frac{r_{11}}{r_{12}} \right)^2 \right)} + 1 \right) \alpha} \right| < 0.22 \quad (31)$$

Finally, the geometrical parameters of the structure are extracted as:

$$a = \frac{e^2 E_f r_{12}}{\pi \hbar^2 \epsilon_{eff} \omega_2^2} \quad (32.a)$$

$$\tau E_f = \alpha \left(\frac{L}{a} \right)^2 \frac{K_2 \pi \hbar^2}{\pi^2 \zeta_2^2 e^2 \eta_0} \quad (32.b)$$

in which, $\zeta_2 = S_2/a$.

In the following, we design the parameters of an absorber to realize a dual-band absorber based on the array of disks. As an example, suppose the second band occurs at $f_2 = 5 \text{ THz}$, the geometrical parameters of the absorber would be as: $a = 2.3 \mu\text{m}$, $L = 5.1 \mu\text{m}$ and $h = 4.8 \mu\text{m}$. The properties of graphene are driven as $\tau = 2.2 \text{ ps}$ and $E_f = 0.38 \text{ eV}$. For designing this absorber, $\alpha = 0.8$ is considered to do the calculations which satisfy Eq. 31. The analytical results are verified by the results obtained by full-wave simulations carried out by HFSS. The absorption of such structure as the function of the frequency is given in Fig. 7. It can be observed that two absorption bands occur with absorptivity 100% and 95% at first and second bands, respectively. The loss distributions on disks are plotted in Fig.8 at first and second resonant frequencies.

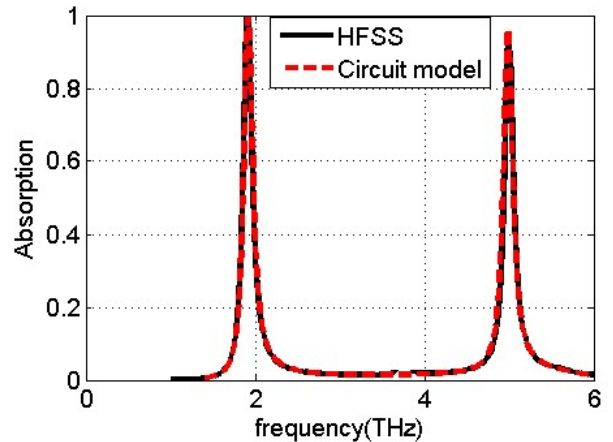


Fig. 7. Absorption spectra of the absorber with configuration plotted in Fig. 6 with parameters $a = 2.3 \mu\text{m}$, $L = 5.13 \mu\text{m}$ and $h = 4.8 \mu\text{m}$. The properties of graphene appear as $\tau = 2.2 \text{ ps}$ and $E_f = 0.38 \text{ eV}$.

Now, the tunability of the proposed device is investigated by changing the Fermi level. The Fermi level of graphene can be regulated in a varied range by altering the bias voltage.

Fig. 8 shows the absorption spectra for the Fermi level range between 0.4 eV to 0.6 eV. It can be observed that the first resonant frequency is slightly shifted to higher frequencies with increasing the Fermi level where the variations of its resonant peak are considerable. However, the changes of the location of the second resonant band are significant while its absorption peak slightly decreases and for the range between 0.45 eV to 0.55 eV is approximately constant.

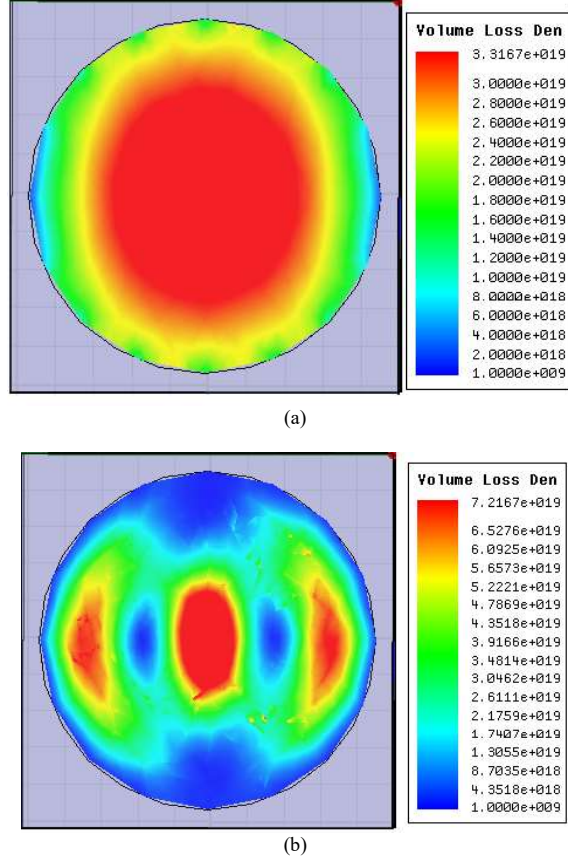


Fig. 7 The loss density distributions on the graphene disks at both resonant frequencies of Fig.6.

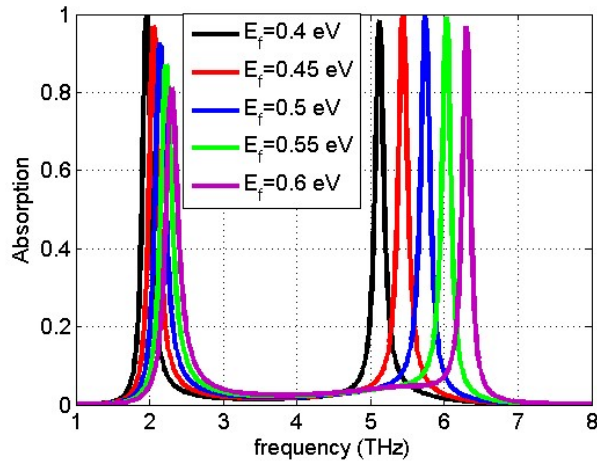


Fig. 8 Absorption spectra of the graphene-based proposed absorber for different Fermi level of graphene.

To survey the influence of incident angle on the absorption properties of the proposed absorber, we simulate the absorption spectra for different incident angle as plotted in Fig. 9. It can be observed, for the incident angle below 40, both resonant frequencies with absorption level above 90% remain for both TE and TM polarizations. For TM polarization, the first resonant band keeps a great absorption level for all incident angles but the absorption level decrease for the second band with increasing the incident angle. For TE polarization, the absorption level of the first band gradually decreases when the incident angle increases but however the second band keeps a great absorption level for all incident angles.

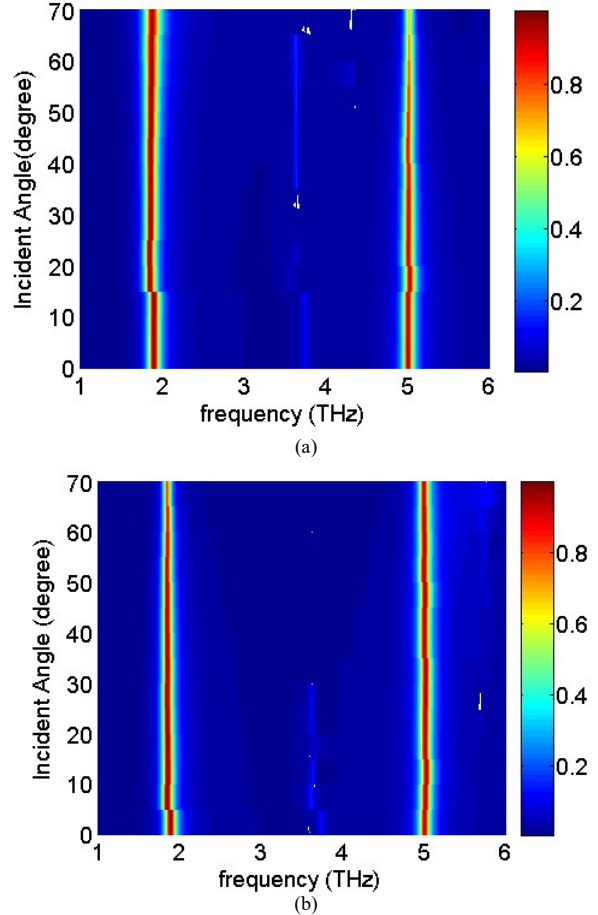


Fig. 9 Absorption spectra of the graphene-based absorber as function of incident angle and frequency for (a) TM and (b) TE polarizations.

4. Conclusion

In the current study, dual-band absorbers based on graphene ribbons and disks deposited above a grounded dielectric slab have been designed for low terahertz regimes. The design was using exciting two first GPPs to achieve two absorption bands. The circuit models including two parallel branches of the R-L-C series circuits describing these GPPs have been used to analytically design the proposed absorber. We obtained the closed form relations for geometrical parameters and properties of graphene. The loss distributions at each resonance showed that a GPP has been excited at each resonant band. The results indicated that the

resonant bands of the proposed absorber are adjustable by changing the geometrical parameters and The Fermi level. In addition, it had been demonstrate the absorber based on graphene disks is polarization insensitive and wide angle. Furthermore, the resonant bands of the proposed absorbers were very narrow band.

5. References

- [1] D. K. Gramotnev and S. I. Bozhevolnyi, "Plasmonics beyond the diffraction limit," *Nat. Photonics*, vol.4, pp.83-91, 2010.
- [2] S. Xiao, and N. A. Mortensen, "Surface-plasmon-polariton-induced suppressed transmission through ultrathin metal disk arrays," *Opt. Lett.*, vol. 36, pp. 37, 2011.
- [3] D. K. Gramotnev and S. I. Bozhevolnyi, "Nanofocusing of electromagnetic radiation," *Nat. Photonics*, vol. 8, pp. 13, 2014.
- [4] S. Farazi and A. Zarifkar, "Ultrafast and low-power plasmon-soliton switching based on two-dimensional MoS₂ nanostructure," *J. Opt. Soc. Am. B*, vol. 34, pp. 2238-2243, 2017.
- [5] B. Janjan, D. Fathi, M. Miri, and M. Ghaffari-Miab, "Ultra-wideband high-speed Mach-Zehnder switch based on hybrid plasmonic waveguides," *Appl. Opt.*, vol. 56, pp. 1717-1723, 2017.
- [6] F. Hu and Z. Zhou, "Wavelength filtering and demultiplexing structure based on aperture-coupled plasmonic slot cavities," *J. Opt. Soc. Am. B*, vol. 28, pp. 2518-2523, 2011.
- [7] C. T. Wu, C. C. Huang, and Y. C. Lee, "Plasmonic wavelength demultiplexer with a ring resonator using high-order resonant modes," *Appl. Opt.*, vol. 56, pp. 4039-4044, 2017.
- [8] H. A. Atwater and A. Polman, "Plasmonics for improved photovoltaic devices," *Nat. Mater.*, vol. 9, pp. 205, 2010.
- [9] S. Xiao, E. Stassen, and N. A. Mortensen, "Ultra thin silicon solar cells with enhanced photo current assisted by plasmonic nanostructures," *J. Nanophot.*, vol. 6, pp. 061503, 2012.
- [10] S. Xiao, X. Zhu, B. Li, and N. Asger, "Graphene-plasmon polaritons: from fundamental properties to potential applications," *Frontiers of Physics*, vol. 11, pp. 117801, 2016.
- [11] Q. Bao and K. P. Loh, "Graphene photonics, plasmonics, and broadband optoelectronic devices," *ACS Nano*, vol. 6, no. 5, pp. 3677-3694, 2012.
- [12] F. Wang et al., "Gate-variable optical transitions in graphene," *Science*, vol. 320, no. 5873, pp. 206-209, 2008.
- [13] F. H. Koppens, D. E. Chang, and F. J. G. de Abajo, "Graphene plasmonics: A platform for strong light-matter interactions," *Nano Lett.*, vol. 11, no. 8, pp. 3370-3377, 2011.
- [14] F. Xia, T. Mueller, Y. Lin, A. Valdes-Garcia, and P. Avouris, "Ultrafast graphene photodetector," *Nature Nanotechnol.*, vol. 4, no. 12, pp. 839-843, 2009.
- [15] H. Raether, *Surface Plasmons on Smooth and Rough Surfaces on Gratings*, Berlin: Springer, 1988.
- [16] Y. Ding, X. Zhu, S. Xiao, H. Hu, L. H. Frandsen, N. A. Mortensen, and K. Yvind, "Effective electro-optical modulation with high extinction ratio by a graphene-silicon microring resonator," *Nano Lett.*, vol. 15, no. 7, pp. 4393, 2015.
- [17] C. T. Phare, Y.-H. D. Lee, J. Cardenas, and M. Lipson, "Graphene electro-optic modulator with 30 GHz bandwidth," *Nat. Photonics* 9, 511 (2015)
- [18] I. Goykhman, U. Sassi, B. Desiatov, N. Mazurski, S. Milana, D. de Fazio, A. Eiden, J. Khurgin, J. Shappir, U. Levy, and A. C. Ferrari, "On-chip integrated, silicon-graphene plasmonic Schottky photodetector, with high responsivity and avalanche photo gain," arXiv: 1512.08153
- [19] B. Sensale-Rodriguez, R. Yan, M. M. Kelly, T. Fang, K. Tahy, W. S. Hwang, D. Jena, L. Liu, and H. G. Xing, "Broadband graphene terahertz modulators enabled by intraband transitions," *Nat. Commun.*, vol. 3, pp. 780, 2012.
- [20] M. Liu, X. Yin, E. Ulin-Avila, B. Geng, T. Zentgraf, L. Ju, F. Wang, and X. Zhang, "A graphene-based broadband optical modulator," *Nature*, vol. 474, p. 64, 2011.
- [21] G. Liang, X. Hu, X. Yu, Y. Shen, L. H. Li, A. G. Davies, E. H. Linfield, H. K. Liang, Y. Zhang, S. F. Yu, and Q. J. Wang, "Integrated terahertz graphene modulator with 100% modulation depth," *ACS Photonics*, vol.2, no.11, p. 1559, 2015.
- [22] C. Liang, G. Niu, X. Chen, Z. Zhou, Z. Yi, X. Ye, T. Duan, Y. Yi, and S. Xiao, "Tunable triple-band graphene refractive index sensor with good angle-polarization tolerance," *Opt. Commun.*, vol. 436, p. 57, 2019.
- [23] C. Cen, H. Lin, J. Huang, C. Liang, X. Chen, Y. Tang, Z. Yi, X. Ye, J. Liu, Y. Yi, and S. Xiao, "A Tunable Plasmonic Refractive Index Sensor with Nanoring-Strip Graphene Arrays," *Sensors*, vol.18, p. 4489, 2018.
- [24] J. N. Anker, W. P. Hall, O. Lyandres, N. C. Shah, J. Zhao, and R. P. Van Duyne, "Biosensing with plasmonic nanosensors," *Nat. Mater.*, vol. 7, no. 6, p. 442, 2008.
- [25] A. Marini, I. Silveiro, and F. J. Garc'ia de Abajo, "Molecular sensing with tunable graphene plasmons," *ACS Photonics*, vol. 2, no. 7, p. 876, 2015.
- [26] D. Rodrigo, O. Limaj, D. Janner, D. Etezadi, F. J. Garc'ia de Abajo, V. Pruneri, and H. Altug, "Mid-infrared plasmonic biosensing with graphene," *Science*, vol. 349. no. 6244, p. 165, 2015.
- [27] M. Biabanifard, S. Asgari, S. Biabanifard, and M. S. Abrishamian, "Analytical design of tunable multi-band terahertz absorber composed of graphene disks," *Optik*, vol. 182, 433-442, 2019.
- [28] S. Biabanifard, M. Biabanifard, S. Asgari, Sh. Asadi, and M. C. E. yagoub, "Tunable ultra-wideband terahertz absorber based on graphene disks and ribbons," *Optics Communications*, vol. 427, 418-425, 2018.
- [29] M. Biabanifard, and M. S. Abrishamian, "Circuit modeling of tunable terahertz graphene absorber," *Optik*, vol. 158, 842-849, 2018.
- [30] B. Xiao, M. Gu, and S. Xiao, "Broadband, wide-angle and tunable terahertz absorber based on cross-shaped graphene arrays," *Applied Optics*, vol. 56, 5458-5462, 2017.
- [31] Y. Cheng, H. Zou, J. Yang, X. Mao, and R. Gong, "Dual and broadband terahertz metamaterial absorber based on a compact resonator structure", *Optical Materials Express*, vol. 8, pp. 3104-3114, 2018.
- [32] Y. Z. Cheng, M. L. Huang, H. R. Chen, Z. Z. Guo, X. S. Mao, and R. Z. Gong, "Ultrathin Six-Band Polarization-Insensitive Perfect Metamaterial Absorber Based on a Cross-Cave Patch Resonator for Terahertz Waves," *Materials*, vol. 10, p. 591, 2017.
- [33] M. Huang, Y. Cheng, Z. Cheng, H. Chen, X. Mao, and R. Gong, "Based on graphene tunable dual-band terahertz metamaterial absorber with wide-angle," *Optics Communications*, vol. 415, pp. 194-201, 2018.
- [34] M. L. Huang, Y. Z. Cheng, Z. Z. Cheng, H. R. Chen, X. S. Mao, and R. Z. Gong, "Design of a Broadband Tunable Terahertz Metamaterial Absorber Based on Complementary Structural Graphene," *Materials*, vol. 11, p. 540, 2018.
- [35] K. Arik, S. AbdollahRamezani, and A. Khavasi, "Polarization insensitive and broadband terahertz absorber using graphene disks," *Plasmonics*, vol. 12, no. 2, pp. 393-398, 2016.
- [36] K. Arik, S. Abdollahramezani, S. Farajollahi, A. Khavasi, and B. Rejaei, "Design of mid-infrared ultra-wideband metallic absorber based on circuit theory," *Optics Communications*, vol. 381, pp. 309-318, 2016.
- [37] A. Khavasi, "Design of ultra-broadband graphene absorber using circuit theory," *J. Opt. Soc. Am. B*, vol. 32, p. 1941, 2015.
- [38] S. Barzegar-Parizi, "Realization of wide-Angle and wideband absorber using metallic and graphene-based metasurface for mid-infrared and low THz frequency," *Opt Quant Electron.*, vol. 50, p. 378, 2018.
- [39] S. Barzegar-Parizi, and A. Khavasi, "Designing dual-Band absorbers by graphene/metallic metasurfaces," *IEEE Journal of Quantum Electronics*, vol. 55, p. 7300108, 2019.

- [40] S. Barzegar-Parizi, "Graphene-based Tunable Dual-Band Absorbers by Ribbon/Disk Array," *Opt Quant Electron.*, vol. 51, p. 167, 2018.
- [41] H. A. Atwater and A. Polman, "Plasmonics for improved photovoltaic devices," *Nat. Mater.*, vol. 9, pp. 205-213, 2011.
- [42] R. A. Pala, J. White, E. Barnard, J. Liu, M. L. Brongersma, "Design of plasmonic thin-film solar cells with broadband absorption enhancements" *Adv Mater*, vol. 21, pp. 3504-3509, 2009.
- [43] N. Liu, M. Mesch, T. Weiss, M. Hentschel, and H. Giessen, "Infrared perfect absorber and its Application as plasmonic sensor" *Nano Lett*, vol. 10, pp. 2342-2348, 2010.
- [44] T. Maier, and H. Brückl, "Wavelength-tunable microbolometers with metamaterial absorbers," *Opt. Lett.*, vol. 34, p. 3012, 2009.
- [45] X. Liu, T. Starr, A. F. Starr, and W. J. Padilla, "Infrared spatial and frequency selective metamaterial with near-unity absorbance," *Phys. Rev. Lett.*, vol. 104, p. 207403, 2010.
- [46] X. Liu, T. Tyler, T. Starr, A. F. Starr, N. M. Jokerst, and W. J. Padilla, "Taming the blackbody with infrared metamaterials as selective thermal emitters," *Phys. Rev. Lett.*, vol. 107, no. 4, 045901, 2011.
- [47] A. Khavasi, B. Rejaei, "Analytical modeling of graphene ribbons as optical circuit elements," *IEEE Journal of Quantum Electronics*, vol. 50, pp. 397-403, 2014.
- [48] S. Barzegar-Parizi, B. Rejaei, A. Khavasi, Analytical circuit model for periodic arrays of graphene disks, *IEEE Journal of Quantum Electronics*, vol. 51, p. 7000507, 2015.
- [49] S. Barzegar-Parizi, M. -R. Tavakol, and A. Khavasi, "Deriving surface impedance for 2-D arrays of graphene patches using a variational method," *IEEE Journal of Quantum Electronics*, vol. 53, p. 7000106, 2017.
- [50] S. Kim, M. S. Jang, V. W. Brar, K. W. Mauser, and H. A. Atwater, "Electronically tunable perfect absorption in graphene," *Nano Lett*, vol. 18, pp. 971-979, 2018.
- [51] L. Ju, B. Geng, J. Horng, C. Girit, M. Martin, Z. Hao, H. A. Bechtel, X. Liang, A. Zettl, and Y. R. Shen, "Graphene plasmonics for tunable terahertz metamaterials," *Nat. Nanotechnol*, vol. 6, pp. 630-634, 2011.
- [52] C. Dean, A. Young, I. Meric, C. Lee, L. Wang, S. Sorgenfrei, K. Watanabe, T. Taniguchi, P. Kim, and K. Shepard, "Boron nitride substrates for high-quality graphene electronics," *Nat. Nanotechnol.*, vol. 5, pp. 722-726, 2010.
- [53] K. I. Bolotin, K. J. Sikes, Z. Jiang, M. Klima, G. Fudenberg, J. Hone, P. Kim, and H. L. Stormer, "Ultrahigh electron mobility in suspended graphene," *Solid State Commun.*, vol. 146, pp. 351-355, 2008.